This paper was published in Geothermics,
doi:10.1016/j.geothermics.2014.07.002.

Large magnitude events during injections in geothermal reservoirs and hydraulic energy: A heuristic approach

Clément Baujard*[1], Martin Schoenball[2], Thomas Kohl[2], and Louis Dorbath[3]

[1] *Geowatt AG, Zürich, Switzerland*
[2] *Karlsruhe Institute of Technology, Institute of Applied Geosciences, Karlsruhe, Germany*
[3] *Ecole et Observatoire des Sciences de la Terre, Université de Strasbourg, Strasbourg, France*

Abstract

The occurrence of induced seismicity during reservoir stimulation requires robust real-time monitoring and forecasting methods for risk mitigation. We propose to derive an estimation of M_{max} (here defined as the largest single seismic event occurring during or after reservoir stimulation) using hydraulic energy as a proxy to forecast the total induced seismic moment and to model the transient evolution of the seismic moment distribution (based on the Gutenberg-Richter relation). The study is applied to the vast dataset assembled at the European pilot research project at Soultz-sous-Forêts (Alsace, France), where four major hydraulic stimulations were conducted at 5 km depth. Although the model could reproduce the transient evolution trend of M_{max} for every dataset, detailed results show different agreement with the observations from well to well. This might reveal the importance of mechanical and geological conditions that may show strong local variations in the same EGS.

1 Introduction

Induced seismicity is a crucial issue for Enhanced Geothermal Systems (EGS) development. Large magnitude events (in the following defined as events showing a moment magnitude larger than 2) can occur during the stimulation phase of the reservoir or during the operational (circulation) phase. Such events were observed in many EGS: in Soultz-sous-Forts, France (Gérard et al., 2006;

*clement.baujard@es-groupe.fr

Charléty et al., 2007; Dorbath et al., 2009) , in Basel, Switzerland (Häring et al., 2008), or in Cooper Basin, Australia (Baisch et al., 2006) for example. In the following, we will focus on seismic events observed during the reservoir development only, i.e. during stimulation phases (during and after injection) conducted by high pressure injections of water or brine. We restrict our analysis to the stimulation phase as it is generally associated with high seismicity rates, which helps to reduce the statistical uncertainty, e.g. compared to the lower seismic activity during long-term production. Our study is based on monitoring data acquired during the stimulation of the 5 km deep boreholes of the EGS of Soultz-sous-Forts (France). Seismicity prediction in geothermal reservoirs using several methods has been developed for years (Baujard, 2003; Kohl and Mégel, 2007). Reservoir models are based on the numerical simulation of physical processes occurring during injection or circulation. Flow in porous and fractured media, mechanical coupling and thermal transport are the most important ones. Examples of such models are FRACTure (Kohl and Hopkirk, 1995), Tough2 (Rutqvist, 2011), or FRACAS (Bruel, 2005). Seismic events magnitudes were successfully simulated using e.g. rate- and state-dependent friction models (McClure and Horne, 2012), block-slider mechanisms (Baisch et al., 2010), discrete particle models (Yoon et al., 2014) or by combining probabilistic approach and empirical observation (Bachmann et al., 2011; Shapiro et al., 2007; Shapiro and Dinske, 2009). Goertz-Allmann and Wiemer (2013) present a model that may explain the observed variation of b-value. It has been showed that cyclic pressurization of a geothermal reservoir could enhance permeability and reduces induced seismicity (Zang et al., 2013). Our work aims at developing a heuristic model that can give indications on the largest magnitude event M_{max} that could be induced during a given pumping sequence in a reservoir. To that purpose, we propose to correlate the hydraulic energy provided to the reservoir by fluid injection and the seismic moment released by induced seismicity, and to use this correlation to derive a prediction of M_{max}, using a real-time Gutenberg-Richter relation computation. Such methods were already applied, as one can find in the literature examples of comparison of the pumped energy, or of the injected volume with the highest magnitude event obtained or with the total seismic moment (see for example McGarr, 1976; Baisch et al., 2009b; McGarr, 2014). Here, we propose to go one step further and to use a simple relation between the hydraulic energy and the total induced seismic moment in order to predict M_{max} evolution during reservoir stimulations resolved by time bins.

2 Physical background

The hydraulic energy applied to a reservoir can be estimated through the integration of pumping power over time or through the integration of the pressure distribution in the reservoir over its volume. The pumped hydraulic energy can be computed with:

$$E_{h,pumped} = \int Q \Delta P dt, \tag{1}$$

with $E_{h,pumped}$ [J] being the pumped hydraulic energy, Q [m^3/s] the flowrate, ΔP [Pa] the overpressure and t [s] the injection time. The integration of the overpressure distribution over the reservoir volume also represents a quantity of energy. The advantage of this estimation of energy is that, on the contrary to the pumping energy (which is zero if computed in a time interval after shut-in), there is still some residual energy after shutting in the well. This energy will be called in the following reservoir hydraulic energy and can be computed with the following relation:

$$E_{h,res} = \iiint \Delta P dV, \tag{2}$$

with E_h, res [J] being the hydraulic reservoir energy, ΔP [Pa] the overpressure and V [m^3] the reservoir (rock and fluid) volume. The seismic moment is obtained by:

$$M_0 = \mu S d \tag{3}$$

with M_0 [Nm] being the seismic moment, μ [Pa] the shear modulus, S [m^2] the surface of rupture and d [m] the displacement. The moment magnitude of the events is computed using the following relation (Hanks and Kanamori, 1979):

$$M_w = \frac{2}{3}\log(M_0)6.07. \tag{4}$$

With M_w [-] being the moment magnitude and M_0 [Nm] the seismic moment.

3 Dataset

Our work is based on the unique data set acquired from the three deep boreholes of the European research pilot-EGS site at Soultz-sous-Forts, France (Dorbath et al., 2009). The following data will be used:

- GPK2 stimulation, starting 30.06.2000. Approx. 23 400 m^3 of water were injected during 6 days. A total number of 6 947 seismic events were recorded and located by a surface network. The highest magnitude recorded was 2.6.
- GPK3 stimulation, starting 27.05.2003. Approx. 37 500 m^3 were injected during 11 days. A total number of 7 175 events were recorded. Only 2 253 events were located. The highest magnitude recorded was 2.9.
- GPK4 first stimulation, starting 13.09.2004. Approx. 9 300 m^3 were injected during 3.5 days. A total of 1 182 events were recorded. Only 794 events were located. The highest magnitude recorded was 2.3.
- GPK4 second stimulation, starting 09.02.2005. Approx. 12 500 m^3 were injected during 4 days. A total of 1 246 events were recorded. Only 764 events were located. The highest magnitude recorded was 2.7.

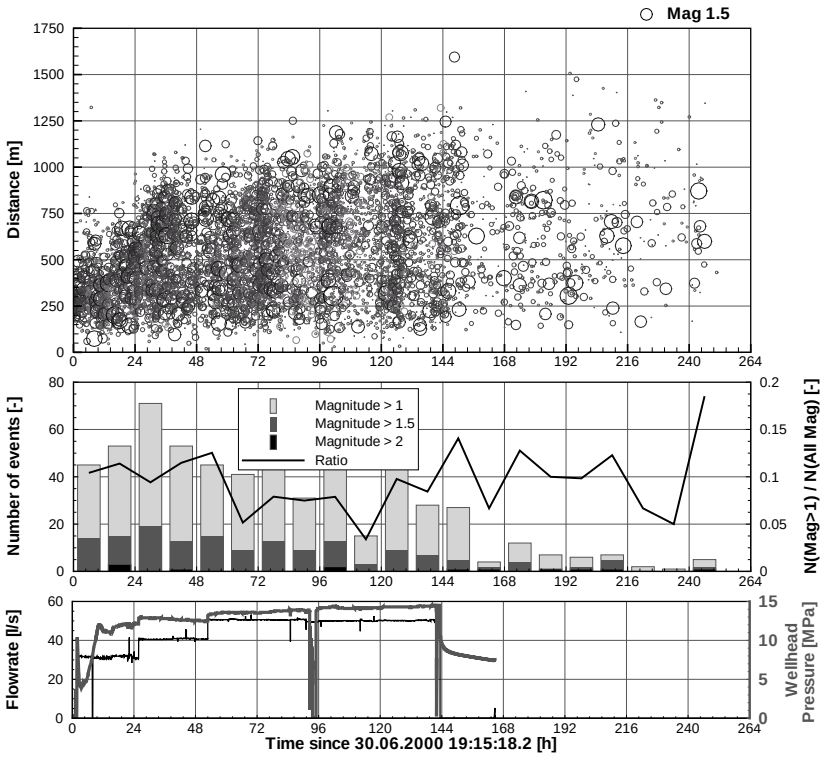

Figure 1: Hydraulic stimulation data of GPK2, 2000. From bottom to top: imposed flowrate and wellhead pressure, event rate and ratio of the number of events of magnitude greater than 1 over the total number of events using 12 hours bins, and distance vs. time of the seismic events with symbol size proportional to magnitude.

These data were acquired using the surface network of EOST (Ecole et Observatoire des Sciences de la Terre - University of Strasbourg). It consisted of 14 temporary stations in 2000, and was upgraded through the installation of nine permanent stations in 2003. For the stimulations in 2004 and 2005 the permanent network was enhanced by a temporary network of only six temporary stations (Dorbath et al., 2009). It must be underlined that the catalogs for GPK4 might be incomplete. The injection scheme considered for each stimulation sequence as well as the time-distance representation for the localized events are represented in figure 1 for the stimulation of GPK2, in figure 2 for GPK3, in figures 3 and 4 for the stimulations of GPK4.

For each injection sequence, an event rate has been calculated for the largest magnitude events (in number of events of magnitude higher than 1, 1.5 and 2 using 12 hours intervals). The ratio of the number of events of magnitude greater than 1 over the total event number was also computed. It can be observed

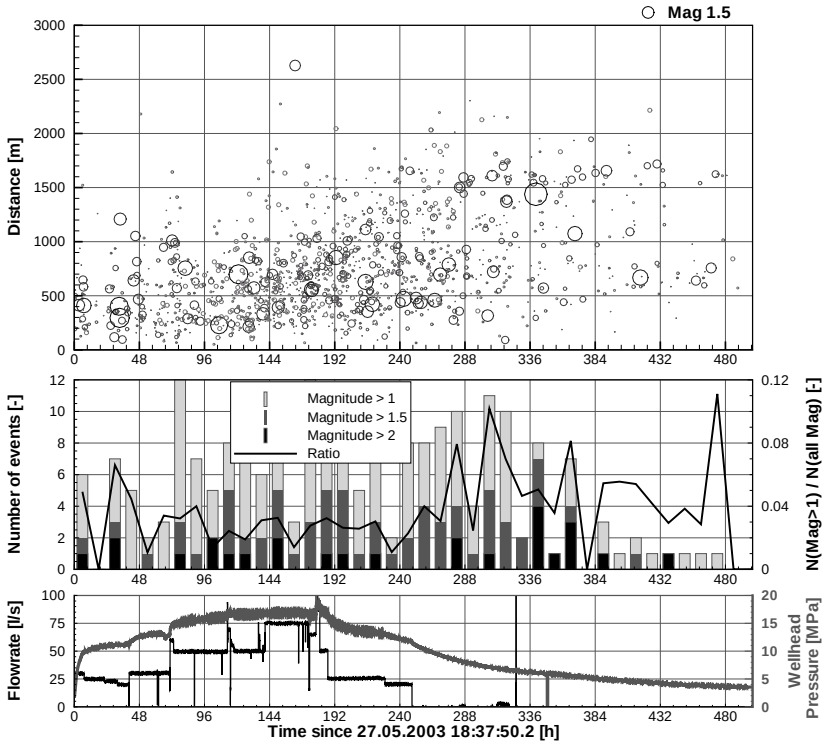

Figure 2: Hydraulic stimulation data of GPK3, 2003. From bottom to top: imposed flowrate and wellhead pressure, event rate and ratio of the number of events of magnitude greater than 1 over the total number of events using 12 hours bins, and distance vs. time of the seismic events with symbol size proportional to magnitude.

that the ratio has a tendency to increase after the shut-in of the well, so the proportion of larger events increases. Similar observations have been made by Schindler et al. (2008), who found that the mean amplitudes recorded at the seismic stations increased significantly after shut-in. Furthermore, there are numerous examples where the largest event induced by hydraulic stimulation was observed after shut-in (Baisch et al., 2006, 2009b; Häring et al., 2008). It was also shown, that the b-value tends to decrease after shut-in (Bachmann et al., 2011), which results in a larger proportion of large magnitude events.

The total energy pumped into the system during the pumping sequence and the total seismic moment have been calculated for each stimulation (see table 1 and figure 5). The total seismic moment is the sum of the seismic moments of all events. Deriving a universal relation between the total seismic moment and the pumped energy is not possible using simple physical considerations. Nevertheless, as it seems that the total seismic moment increases with the pumped

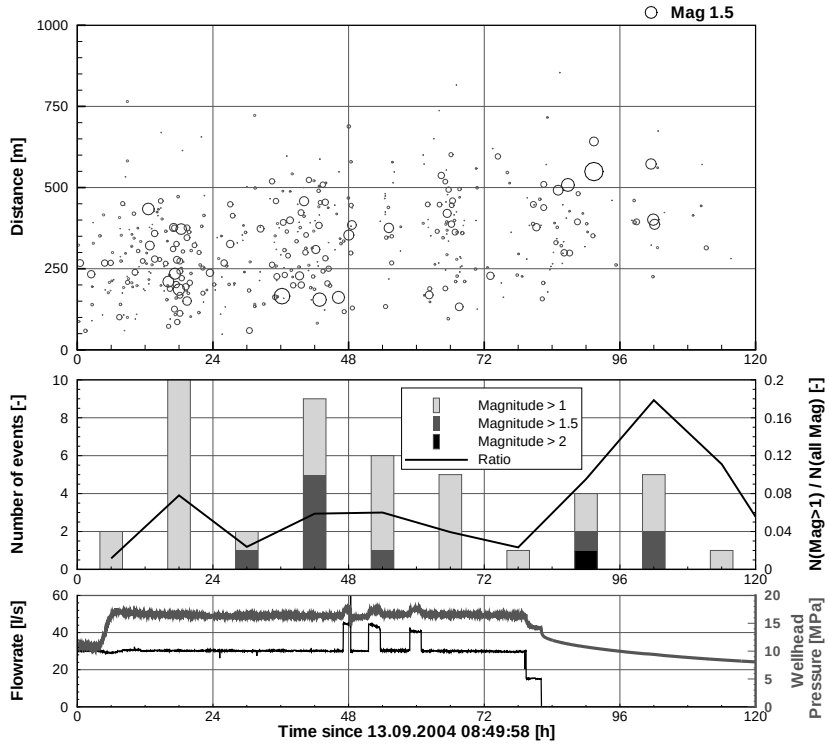

Figure 3: Hydraulic stimulation data of GPK4, 2004. From bottom to top: imposed flowrate and wellhead pressure, events rate and ratio of the number of events of magnitude greater than one over the total events number using 12 hours bins, and distance vs. time of the seismic events.

energy, an empirical linear relation will be assumed in the following between hydraulic energy and total seismic moment released, as follows:

$$M_0 = cE_h \tag{5}$$

With M_0 [Nm] the seismic moment, E_h [J] the hydraulic energy, and c a constant.

4 Methodology

The proposed methodology aims at predicting the total seismic moment that will be released at time t+ t, using a comparison between the hydraulic energy injected into the system and the total seismic moment released at time t. The general methodology can be summarized by the following steps:

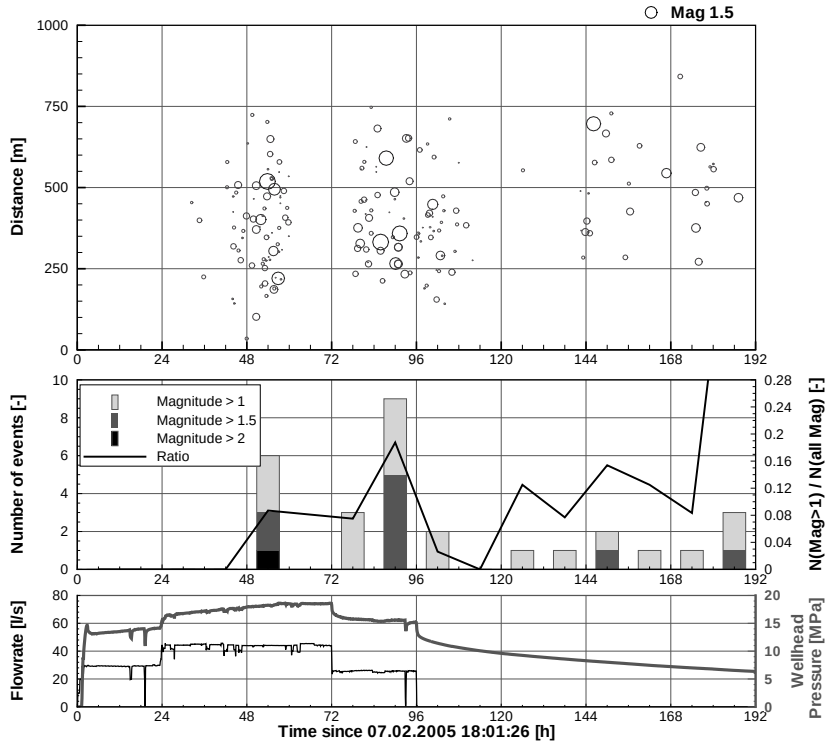

Figure 4: Hydraulic stimulation data of GPK4, 2005 (right). From bottom to top: imposed flowrate and wellhead pressure, events rate and ratio of the number of events of magnitude greater than one over the total events number using 12 hours bins, and distance vs. time of the seismic events.

- Step 1: at time t, computation of the ratio R of total seismic moment recorded $M_{0,t}$ [Nm] and the hydraulic energy injected $E_{h,t}$ [J]:

$$R = \frac{M_{0,t}}{E_{h,t}} \tag{6}$$

- Step 2: at time t, the b-value is computed, following the Gutenberg-Richter relation (Gutenberg and Richter, 1944). The value of the seismic moment obtained for $N = 1$ and $N = 10$ is computed, where N is the events number of a given magnitude.

- Step 3: at time $t + \Delta t$, the total predicted seismic moment is computed after:

$$M_{0,t+\Delta t} = RE_{h,t+\Delta t} \tag{7}$$

$M_{0,t+\Delta t}$ [Nm] and $E_{h,t+\Delta t}$ [J] being the total seismic moment predicted and the hydraulic energy injected or present in the system at a time $t+\Delta t$,

	Hydraulic Energy		Seismic Moment	
	E_h [J]	$\log E_h$	M_0 [Nm]	$\log M_0$
Stim GPK2 2000	3.00×10^{11}	11.48	1.47×10^{14}	14.17
Stim GPK3 2003	5.50×10^{11}	11.74	1.50×10^{14}	14.18
Stim GPK4 2004	1.47×10^{11}	11.17	1.29×10^{13}	13.11
Stim GPK4 2005	1.99×10^{11}	11.30	3.79×10^{13}	13.58

Table 1: Pumped hydraulic energy and total seismic moment released the for the stimulations of GPK2 (2000), GPK3 (2003), GPK4 (2004) and GPK4 (2005).

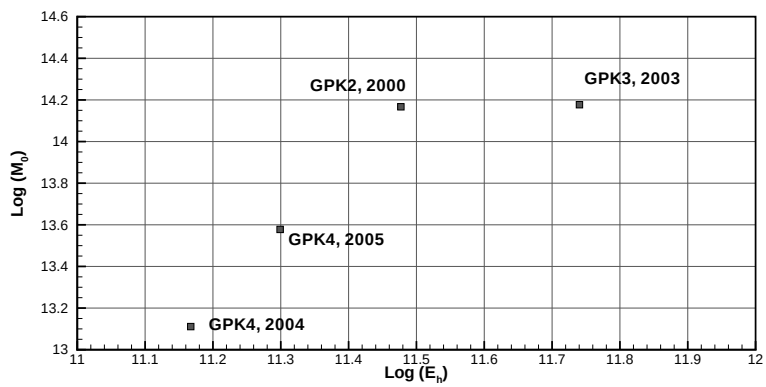

Figure 5: Comparison of the total seismic moment released with the hydraulic pumped energy for the stimulations of GPK2 (2000), GPK3 (2003), GPK4 (2004) and GPK4 (2005).

respectively. Thus, we assume that the hydraulic energy that will be injected into the system during the next phase is known. The way to derive the hydraulic energy will be discussed in more detail in the following.

- Step 4: at time $t + \Delta t$, a new distribution of the predicted seismic events is computed, that fits the predicted total seismic $M_{0,t+\Delta t}$, assuming that the b- value remains the same as during the previous time bin. Thus, it is possible to derive the seismic moment of an event that has a given occurrence. We suggest in the following to take the occurrences N=1 and N=10 as proxies for the determination of M_{max}.

Two models were developed, based on different approaches for estimating hydraulic energy used in eqs. 6 and 7.

4.1 Model 1

In the first model, the ratio R (see eq. 6) is computed by assuming $E_{h,t} = E_{h,pumped}$ and computed after eq. 1. In order to compute the energy at a time

$t + \Delta t$, it is necessary to know the flowrate during Δt, and the corresponding wellhead pressure. In the following, it is assumed that the flowrate is known for the next Δt time interval. The wellhead pressure is predicted assuming that the well injectivity remains constant during the next time interval Δt. The injectivity at a time t is computed after:

$$I_t = \frac{Q_t}{P_t} \tag{8}$$

with Q_t [m^3/s] being the flowrate at a time t and P_t [Pa] the wellhead pressure at a time t. Thus, the pressure at $t + \Delta t$ is computed after:

$$P_{t+\Delta t} = \frac{Q_{t+\Delta t}}{I_t} \tag{9}$$

The main limitation of this model is that hydraulic energy remains constant after the shut-in of the well, as the flowrate drops down to zero. Thus, no prediction can be done for the shut-in phase. According to the number of data available, at a given time t, the seismic moment and the pumped hydraulic energy can be computed from the beginning of the pumping sequence or only for the last period Δt.

4.2 Model 2

In order to predict the seismic response of the reservoir during shut-in phases, another strategy was developed. As described above, the hydraulic energy added to the system can also be obtained by integrating the reservoir overpressure induced by the injection over the reservoir volume. In this model, physical quantities are derived at a reservoir scale. The pressure integration is done over the entire reservoir volume (i.e. the pressurized rock and fluid volume), and not only additional fluid volume. The method assumes that the pressure distribution at a time t and at a time $t+\Delta t$, is known. In this model, the pressure distribution at different times is computed assuming the Dupuit steady-state solution of the diffusion equation (de Marsily, 1986), following an isotropic natural logarithmic decrease of the pressure with distance from the injection, after:

$$P_{res,t}(r) = a \ln \frac{b}{r}, \tag{10}$$

with $P_{res,t}$ [bar] being the reservoir pressure, r [m] being the distance to the borehole, and a and b two constants. An example of the pressure curve is shown in figure 6. The constants a and b are determined by the following boundary conditions: $P_{res,t}(r = r_0) = P_t, r_0$ [m] being the borehole radius and P_t [bar] the injection pressure at a time t, and $P_{res,t}(r = r_{cloud}) =$ constant, r_{cloud} being the radius of the seismic cloud at a time t. The constant is a parameter of the model (usually relatively low, as it is the minimum shearing pressure). This formulation of the pressure distribution in the reservoir implicitly assumes that the reservoir behaves like a porous medium when observed at a large scale. This

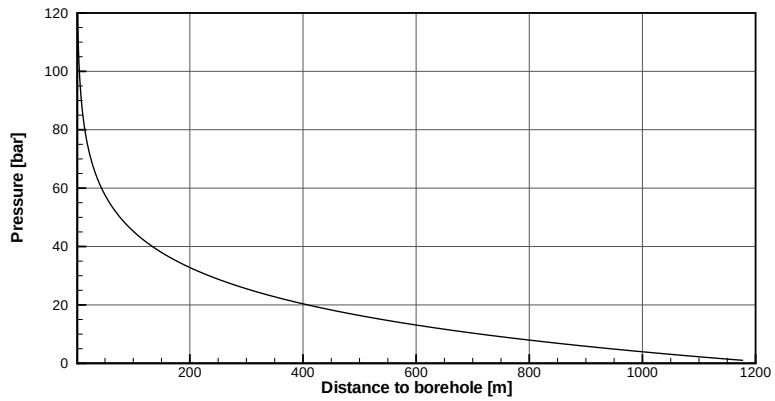

Figure 6: Reservoir pressure model for a wellhead pressure of 120 bar (12 MPa) and a seismic cloud extension of 1 200 m after eq. 9.

assumption is certainly arguable and will be discussed in the last section of this paper. Nevertheless, this formulation will be here accepted as its purpose is to provide a simple analytical solution of the pressure distribution to be integrated in space in order to derive the energy.

In order to be able to compute the reservoir hydraulic energy at a time $t+\Delta t$, one has to know the extension of the cloud at that time. In order to overcome that issue, we propose to compute the seismic diffusivity at a time t, based on the propagation of the triggering front of the hydraulic-induced microseismicity (Shapiro et al., 1999). The extension of the cloud as a time $t + \Delta t$ is then computed after:

$$r_{cloud,t+\Delta t} = \sqrt{4\pi D(t + \Delta t)} \tag{11}$$

With D [m^2/s] being the diffusivity. The diffusivity is fitted using an iteration scheme at every time t, using a tolerance ratio. The diffusivity value is iteratively increased until the envelope drawn by the diffusion equation reaches a tolerance value (see table 2). Thus, it is possible to predict the hydraulic reservoir energy, as one knows at a time $t + \Delta t$ the extension of the cloud as well as the pressure at the borehole (which is derived assuming a constant injectivity, see model 1).

5 Results

Both models need the same input data, which are: hydraulic data: pressure and flowrate with time, seismic data: location and magnitude of events with time The input parameters are the following: the prediction time interval or time bin Δt, a tolerance ratio for the computation of the diffusivity (which is the proportion of events located under the envelope given by eq. 11 for a

Parameter	Value
time interval Δt	12 hours
diffusivity tolerance factor	80 %
magnitude bin length $DeltaM_w$	0.2
magnitude interval for b-value determination	0 - 1.2

Table 2: Model parameters used in the following computations.

given diffusivity) the size of the magnitude bin for the determination of the b-value in the Gutenberg-Richter relation, the magnitude interval used for the determination of the b-value. As the extreme values of magnitude do not follow the Gutenberg-Richter relation (Dorbath et al., 2009), it is necessary to set-up a fixed interval for the determination of the b-value. The influence of these parameters in the computations will be discussed later on in this paper. The parameters used in the following are summarized in table 2. The results obtained for every stimulation campaign are presented in the following. A prediction of the seismic rate and magnitude for the next 12 hours is made every 12 hours. On the following figures, the prediction is shown 12 hours later in order to be compared with the observation. Both models have been run, with the model 1 being limited to the injection sequence. At each time step, the seismic rate and the predicted magnitude of events for occurrence $N = 1$ and $N = 10$ are presented.

GPK2, 2000

The results obtained for the stimulation of GPK2 are shown in figure 7. As the pressure was not monitored after 168 hours (see figure 1), the pressure decrease at the borehole was linearly extrapolated during the next 72 hours in order to allow a prediction. Both models give comparable results. As it can be observed, the predicted seismic rate is well correlated with the observations, for both models. The magnitude of the event with occurrence N=1 is higher than the observed highest magnitude event. The magnitude of the events of occurrence $N = 10$ correlates relatively well with the highest observed magnitude. It must be pointed out that both predicted magnitudes of the event of occurrence $N = 1$ and $N = 10$ do not decrease during the shut-in of the well.

GPK3, 2003

The results obtained for the stimulation of GPK3 are shown in figure 8. Again, both models give comparable results. As for GPK2, the predicted seismic rate is well correlated with the observations, for both models. On the contrary of the GPK2 stimulation, the magnitude of the event with occurrence N=1 gives a realistic prediction of the highest magnitude event that was observed. It is interesting to note that, at the end of the injection (240 hours), the magnitude of the event of occurrence $N = 1$ is 2.8, which seems overestimated in regard

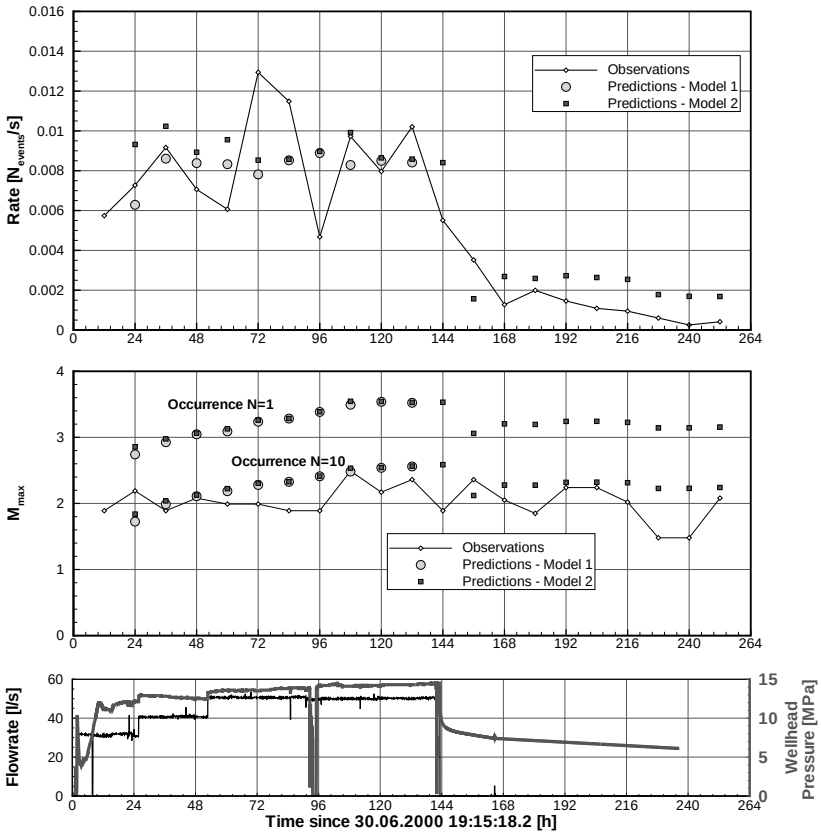

Figure 7: Results of the predictions obtained for the stimulation of GPK2. From bottom to top: imposed flowrate and wellhead pressure, predicted magnitudes of events of occurrence N=1 and N=10, compared with the highest magnitude observed, and predicted seismic events rate compared with the observations.

to the observed highest magnitude events. But, an event of magnitude 2.9 was recorded around 4 days later, i.e. 350 hours after the beginning of the injection.

GPK4, 2004

The results obtained for the stimulation of GPK4 (2004) are shown in figure 9. If the correlation between the predicted seismic events rate and the observations is realistic during the injection, the predicted seismic event rate is overestimated during the shut-in phase of the stimulation. The observed highest magnitude event for each time bin has a very high time variability, making the interpretation of the results of our magnitude prediction relatively problematic. The magnitude of the event of occurrence $N = 1$ ($M_{max} = 2.5$ after 96 hours of injection) corresponds to the largest event observed.

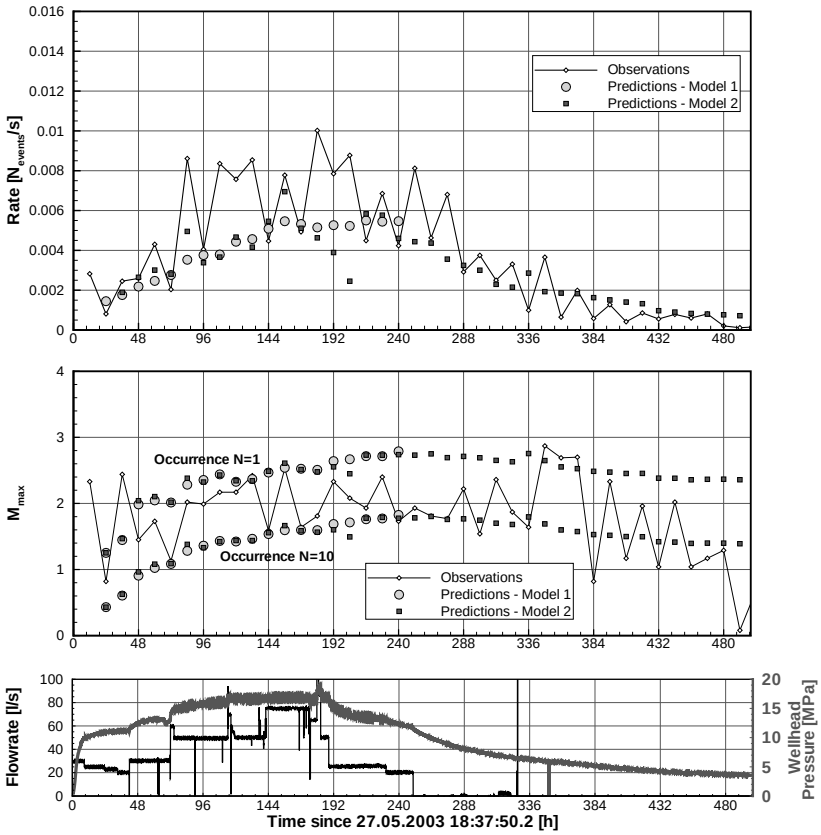

Figure 8: Results of the predictions obtained for the stimulation of GPK3. From bottom to top: imposed flowrate and wellhead pressure, predicted magnitudes of events of occurrence $N = 1$ and $N = 10$, compared with the highest magnitude observed, and predicted seismic events rate compared with the observations.

GPK4, 2005

The results obtained for the second stimulation of GPK4 (2005) are shown in figure 10. The prediction does not correlate very well with the observations. The first prediction of the model can be made only after 50 hours of injections, as the model has to collect enough magnitudes in order to derive a b-value (see also figure 4). The poor quality of the results can be explained by the lack of data recorded during this phase of the stimulation, thus making the determination of a b-value quite problematic. The reason for this anomalous behaviour of the reservoir is the history of the well and a prominent Kaiser effect (see for example Baisch et al., 2009a), that plays a dominant role in the first half of the stimulation. Due to this effect, no seismicity is induced as long as the injection pressure is lower, than the maximum pressure achieved during the

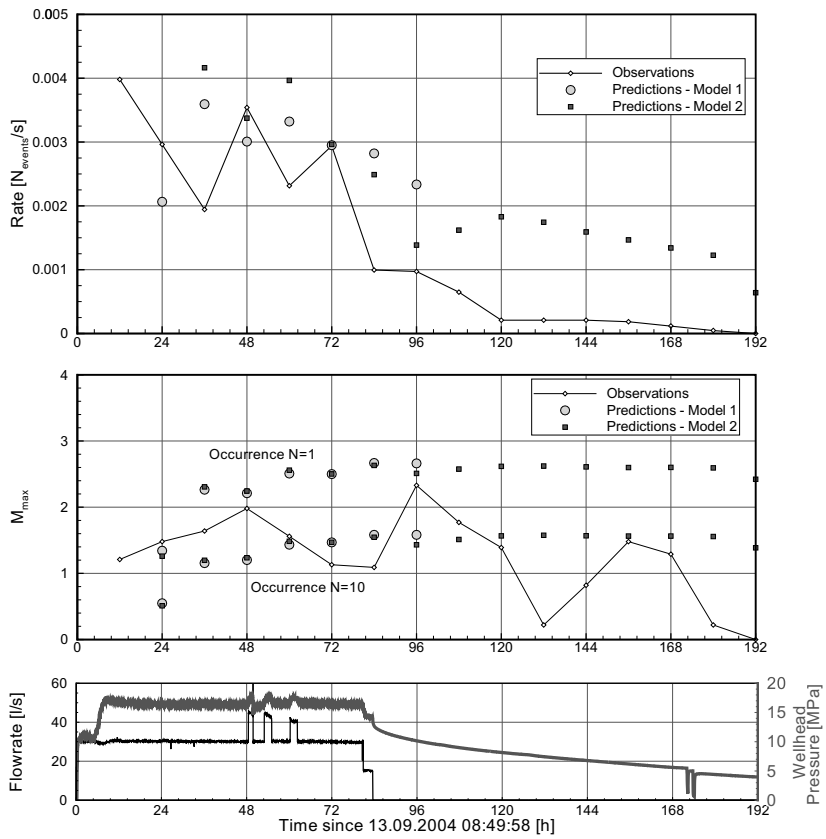

Figure 9: Results of the predictions obtained for GPK4 (2004). From bottom to top: imposed flowrate and wellhead pressure, predicted magnitudes of events of occurrence $N = 1$ and $N = 10$, compared with the highest magnitude observed, and predicted seismic events rate compared with the observations.

first stimulation in 2004.

Summary of the results

The predicted maximum magnitude for every stimulation campaign is shown in the table 3. As can be observed, except for GPK2, the highest predicted magnitude of the events of occurrence $N = 1$ is generally quite close to the highest magnitude observed in reality.

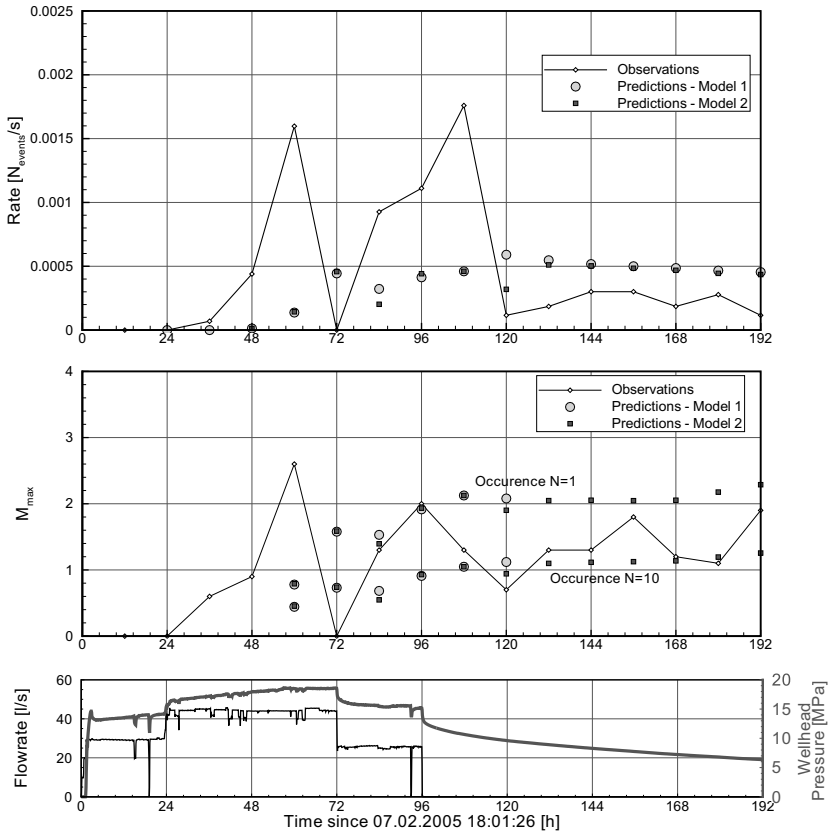

Figure 10: Results of the predictions obtained for GPK4 (2005). From bottom to top: imposed flowrate and wellhead pressure, predicted magnitudes of events of occurrence $N = 1$ and $N = 10$, compared with the highest magnitude observed, and predicted seismic events rate compared with the observations.

	Maximum magnitude of occurrence N=1	Maximum magnitude of occurrence N=10	Largest magnitude observed
GPK2, 2002	3.5	2.6	2.5
GPK3, 2003	2.8	1.8	2.9
GPK4, 2004	2.5	1.6	2.3
GPK4, 2005	2.6	1.3	2.3

Table 3: Comparison of the maximum magnitude of the events of occurrence $N = 1$ and $N = 10$ with the highest magnitude observed

6 Discussion

Several observations can be made on our results. Firstly, it can be observed that the magnitude of the events with occurrence $N = 1$ or $N = 10$ hardly decrease during the shut-in phase, for all wells. This is a consequence of the fact that the hydraulic energy that has been injected into the system only resorbs very slowly after the end of the injection in the datasets used. Also, it must be pointed out that the seismic rate rapidly decreases after the shut- in, thus limiting the risk of obtaining a large magnitude seismic event. On the other hand, b-value decreases after shut-in which in turn increases M_{max}. Secondly, results obtained for GPK2 and GPK3, which are the best datasets available, show very different agreement with the observations. The predictions of the magnitude of the events of occurrence $N = 1$ are much higher than the observed highest magnitude events for GPK2, on the contrary to GPK3, for which the magnitude of the events of occurrence $N = 1$ is quite closed to the observed highest magnitude. Several reasons could explain these different behaviours:

- The lack of large scale structures (faults) in the vicinity of GPK2 (Dorbath et al., 2009; Schoenball et al., 2012). Indeed, an event of magnitude 3.5, which is the predicted magnitude of the events of occurrence $N = 1$ would require a fault of around 500 m diameter. If no such structure is to be found in the neighbourhood of GPK2, no such event could happen.
- In the case of GPK3, it is well established that an important structure has been met in the open section of the well at 4770m depth (Sausse et al., 2010; Held et al., 2014). Thus, this structure may allow movements of large areas and consequently leads to the occurrence of large magnitude seismic events during the stimulation.
- The reservoir structure and rock properties vary from well to well. The open hole section of GPK2 is characterized by a higher clay content than the open hole section of GPK3 (Meller et al., 2014). The clay content is known to be a critical parameter for the failure modes to be brittle, hence seismic, or ductile and aseismic (Tembe et al., 2010).

The sensitivity of the model response to the input parameters has to be mentioned here. In fact, the sensitivity of the model to the time interval Δt, to the tolerance factor for the computation of the diffusivity and to the magnitude bin length ΔM_w is very limited. On the contrary, sensitivity of the model response to the magnitude interval used for the determination of the b- value is relatively high (see figure 11). This parameter has a direct influence on the b-value and thus on the predicted magnitude of the events of different occurrence probabilities. Despite the high sensitivity of the model to this parameter, the advantage of the method here proposed is that the number of user-defined input parameters remains very limited and that no manual data fit is needed. It is therefore suitable for real-time monitoring and prediction of seismic activity during stimulation or operation in geothermal reservoirs.

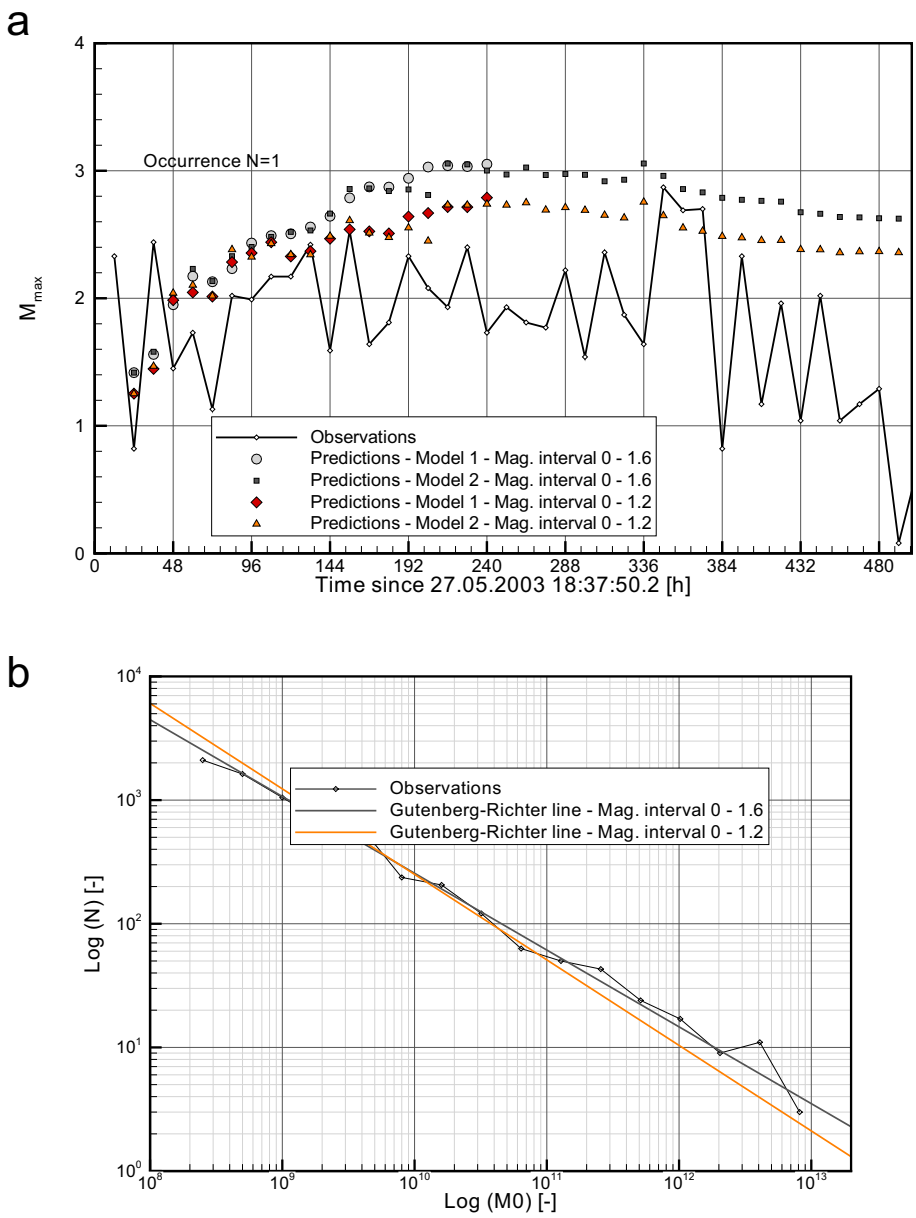

Figure 11: Top: sensitivity of the results to the magnitude interval used for the determination of the b-value (example with GPK3). Bottom: sensitivity of the Gutenberg-Richter law computed at the end of the stimulation.

The presented methodology shows several limitations. The implemented hydraulic model (pressure prediction assuming that injectivity remains constant for the next time bin, and pressure distribution in the reservoir following a Dupuit steady-state) is very simple. Further developments could couple this method with more complex 3D hydro-mechanical models (see for example Kohl et al., 2004). As mentioned with GPK4, the model does not take into account past injections/stimulations. Implementing a reservoir initial state and initial b-value could improve that point. The ability of the models to predict post shut-in seismic activity is limited, as aftershocks (Omori- Utsu seismicity decay) are not taken into account. The spatial variation of b- values, as presented by Goertz-Allmann and Wiemer (2013) could not be taken into account in the models, as well as stress variations occurring into the reservoir (as the stress state of the reservoir is not considered). The presented model cannot take into account aseismic slips that could occur in the reservoir during stimulation. Indications for large-scale aseismic deformations have been obtained from 4D-tomography, revealing strong changes of seismic velocities (Calo et al., 2011). These can be interpreted as strong changes of the stress field. This was underpinned by Schoenball et al. (2014), who found strong changes of the stress regime, that are incompatible with co-seismic stress changes (Schoenball et al., 2012), and therefore must occur aseismically.

7 Conclusions

We presented a heuristic approach to estimate the largest events induced during a reservoir stimulation treatment. Our approach relies on the observation of seismicity, determination of their magnitudes and the past and projected hydraulic schedule for the operation. Since real-time seismic monitoring is standard now, our approach is easy to implement in an action scheme for a planned operation. We use two different models for the calculation of the hydraulic energy. The first one relies on the operational parameters pressure and injection rate. In order to predict the post shut-in phase we use an analytical solution which integrates the pressure perturbation over the reservoir volume. Results of both models are very similar during the injection phases; therefore the applied analytical solution appears to be valid. The models could reproduce the transient evolution trend of M_{max} for every dataset. The predicted seismic rate is well correlated with the observations for all 4 stimulations. The magnitude of the events with a predicted occurrence $N = 10$ gives a realistic prediction of the highest magnitude event that was observed for GPK2, whereas the magnitude of the event with occurrence $N = 1$ correlates relatively well with the highest observed magnitude during GPK3 stimulation. Concerning GPK4 stimulation, the observed highest magnitude event for each time bin shows a strong variability, making the interpretation of the results of our magnitude prediction relatively problematic. For a given dataset, the highest predicted magnitude of the events of occurrence $N = 1$ is generally quite close to the highest magnitude observed in reality. The observed differences of the seismogenic responses be-

tween the stimulation appear to not be solely related to the reservoir treatment, i.e. the energy supplied to the system by fluid injection. Instead, the individual geological conditions for each well at the Soultz reservoir, that is the hydraulic connection to the local fracture network and its mechanical properties, defined e.g. by the clay content plays a critical role.

Acknowledgements

This study was supported by the 7th EU framework programme for Research and Technical Development and carried out within the framework of the GEISER (Geothermal Engineering Integrating Mitigation of Induced Seismicity in Reservoirs) project. The authors would like to thank GEIE Soultz-sous-Forts and specially Nicolas Cuenot for data and ideas exchange.

References

Bachmann, C. E., Wiemer, S., Woessner, J., and Hainzl, S. (2011). Statistical analysis of the induced Basel 2006 earthquake sequence: introducing a probability-based monitoring approach for Enhanced Geothermal Systems. *Geophysical Journal International*, 186(2):793–807.

Baisch, S., Carbon, D., Dannwolf, U., Delacou, B., Devaux, M., Dunand, F., Jung, R., Koller, M., Martin, C., Sartori, M., Secanell, R., and Vörös, R. (2009a). Deep Heat Mining Basel - Seismic Risk Analysis. Technical report, SERIANEX Group, Departement für Wirtschaft, Soziales und Umwelt des Kantons Basel-Stadt, Basel.

Baisch, S., Vörös, R., Rothert, E., Stang, H., Jung, R., and Schellschmidt, R. (2010). A numerical model for fluid injection induced seismicity at Soultz-sous-Forets. *International Journal of Rock Mechanics and Mining Sciences*, 47(3):405–413.

Baisch, S., Weidler, R., Voros, R., Wyborn, D., and de Graaf, L. (2006). Induced seismicity during the stimulation of a geothermal HFR reservoir in the Cooper Basin, Australia. *Bulletin of the Seismological Society of America*, 96(6):2242–2256.

Baisch, S., Weidler, R., Wyborn, D., and Vörös, R. (2009b). Investigation of fault mechanisms during geothemal reservoir stimulation experiments in the Cooper Basin, Australia. *Bulletin of the Seismological Society of America*, 99(1):148–158.

Baujard, C. (2003). *Modélisation de lécoulement de deux fluides non miscibles dans des milieux fracturés; application à linjection deau à grande profondeur et à la recherche deau douce en milieu côtier*. PhD thesis, Paris School of Mines.

Bruel, D. (2005). Using the migration of induced micro-seismicity as a constraint for HDR reservoir modelling. In *30th Stanford Geothermal Workshop*, Stanford, California.

Calo, M., Dorbath, C., Cornet, F. H., and Cuenot, N. (2011). Large-scale aseismic motion identified through 4-D P-wave tomography. *Geophysical Journal International*, 186(3):1295–1314.

Charléty, J., Cuenot, N., Dorbath, L., Dorbath, C., Haessler, H., and Frogneux, M. (2007). Large earthquakes during hydraulic stimulations at the geothermal site of Soultz-sous-Forêts. *International Journal of Rock Mechanics and Mining Sciences*, 44(8):1091–1105.

de Marsily, G. (1986). *Quantitative Hydrogeology, Groundwater Hydrology for Engineers*. Academic Press, Orlando.

Dorbath, L., Cuenot, N., Genter, A., and Frogneux, M. (2009). Seismic response of the fractured and faulted granite of Soultz-sous-Forets (France) to 5 km deep massive water injections. *Geophysical Journal International*, 177(2):653–675.

Gérard, A., Genter, A., Kohl, T., Lutz, P., Rose, P., and Rummel, F. (2006). The deep EGS (Enhanced Geothermal System) project at Soultz-sous-Forets (Alsace, France). *Geothermics*, 35(5-6):473–483.

Goertz-Allmann, B. P. and Wiemer, S. (2013). Geomechanical modeling of induced seismicity source parameters and implications for seismic hazard assessment. *Geophysics*, 78(1):KS25–KS39.

Gutenberg, B. and Richter, C. F. (1944). Frequency of earthquakes in California. *Bulletin of the Seismological Society of America1*, 34:185–188.

Hanks, T. C. and Kanamori, H. (1979). A moment magnitude scale. *Journal of Geophysical Research*, 84(B5):2348.

Häring, M. O., Schanz, U., Ladner, F., and Dyer, B. C. (2008). Characterisation of the Basel 1 enhanced geothermal system. *Geothermics*, 37(5):469–495.

Held, S., Genter, A., Kohl, T., Kölbel, T., Sausse, J., and Schoenball, M. (2014). Economic evaluation of geothermal reservoir performance through modeling the complexity of the operating EGS in Soultz-sous-Forêts. *Geothermics*, 51:270–280.

Kohl, T. and Hopkirk, R. (1995). FRACTure A simulation code for forced fluid flow and transport in fractured, porous rock. *Geothermics*, 24(3):333–343.

Kohl, T. and Mégel, T. (2007). Predictive modeling of reservoir response to hydraulic stimulations at the European EGS site Soultz-sous-Forêts. *International Journal of Rock Mechanics and Mining Sciences*, 44(8):1118–1131.

Kohl, T., Mégel, T., and Baria, R. (2004). Numerical evaluation of massive stimulation experiments. *GRC Transactions*, 28:295–298.

McClure, M. W. and Horne, R. N. (2012). Investigation of injection-induced seismicity using a coupled fluid flow and rate/state friction model. *Geophysics*, 76:WC183.

McGarr, A. (1976). Seismic moments and volume changes. *Journal of Geophysical Research*, 81(8):1487–1494.

McGarr, A. (2014). Maximum magnitude earthquakes induced by fluid injection. *Journal of Geophysical Research: Solid Earth*, 119(2):1008–1019.

Meller, C., Genter, A., and Kohl, T. (2014). The application of a neural network to map clay zones in crystalline rock. *Geophysical Journal International*, 196(2):837–849.

Rutqvist, J. (2011). Status of the TOUGH-FLAC simulator and recent applications related to coupled fluid flow and crustal deformations. *Computers and Geosciences*, 37(6):739–750.

Sausse, J., Dezayes, C., Dorbath, L., Genter, A., and Place, J. (2010). 3D model of fracture zones at Soultz-sous-Forêts based on geological data, image logs, induced microseismicity and vertical seismic profiles. *Comptes Rendus Geoscience*, 342(7-8):531–545.

Schindler, M., Nami, P., Schellschmidt, R., Teza, D., and Tischner, T. (2008). Correlation of hydraulic and seismic observations during stimulation experiments in the 5 km deep crystalline reservoir at Soultz. In *EHDRA scientific conference*, page 8, Soultz-sous-Forêts, France.

Schoenball, M., Baujard, C., Kohl, T., and Dorbath, L. (2012). The role of triggering by static stress transfer during geothermal reservoir stimulation. *Journal of Geophysical Research*, 117(B9):B09307.

Schoenball, M., Sahara, D., and Kohl, T. (2014). Time-dependent brittle creep as a mechanism for time-delayed wellbore failure. *International Journal of Rock Mechanics and Mining Sciences*.

Shapiro, S. A., Audigane, P., and Royer, J.-J. (1999). Large-scale in situ permeability tensor of rocks from induced microseismicity. *Geophysical Journal International*, 137(2):207–213.

Shapiro, S. A. and Dinske, C. (2009). Scaling of seismicity induced by nonlinear fluid-rock interaction. *Journal of Geophysical Research*, 114(B9):B09307.

Shapiro, S. A., Dinske, C., and Kummerow, J. (2007). Probability of a given-magnitude earthquake induced by a fluid injection. *Geophysical Research Letters*, 34(22):1–5.

Tembe, S., Lockner, D. A., and Wong, T.-F. (2010). Effect of clay content and mineralogy on frictional sliding behavior of simulated gouges: Binary and ternary mixtures of quartz, illite, and montmorillonite. *Journal of Geophysical Research*, 115(B3):B03416.

Yoon, J. S., Zang, A., and Stephansson, O. (2014). Numerical investigation on optimized stimulation of intact and naturally fractured deep geothermal reservoirs using hydro-mechanical coupled discrete particles joints model. *Geothermics*.

Zang, A., Yoon, J. S., Stephansson, O., and Heidbach, O. (2013). Fatigue hydraulic fracturing by cyclic reservoir treatment enhances permeability and reduces induced seismicity. *Geophysical Journal International*, 195(2):1282–1287.